



# Glyphosate binding and speciation at the water-goethite interface: A surface complexation model consistent with IR spectroscopy and MO/DFT

Bram Geysels<sup>\*,a,b</sup>, Tjisse Hiemstra<sup>a</sup>, Jan E. Groenenberg<sup>a</sup>, Rob N.J. Comans<sup>a</sup>

<sup>a</sup> Soil Chemistry and Chemical Soil Quality Group, Wageningen University & Research, PO BOX 47, Wageningen 6700 AA, the Netherlands

<sup>b</sup> INVITE GmbH, Otto-Bayer-Straße 32, D-51061 Cologne, Germany

## ARTICLE INFO

### Keywords:

Goethite  
Glyphosate  
Surface speciation  
CD-MUSIC modeling  
MO/DFT  
B3LYP  
@B97X-D  
@B97M-V

## ABSTRACT

Binding of glyphosate (PMG) to metal (hydr)oxides controls its availability and mobility in natural waters and soils, and these minerals are often suggested for the removal of PMG from wastewaters. However, a solid mechanistic and quantitative description of the adsorption behavior and surface speciation on these surfaces is still lacking, while it is essential for understanding PMG behavior in aquatic and terrestrial systems. This study gives new insights through advanced surface complexation modeling of new and previously published adsorption data, supplemented with MO/DFT calculations of the geometry, thermochemistry and theoretical infrared (IR) spectra of the surface complexes. PMG complexation by goethite (FeOOH) was measured over a wide range of pH (~4–10), solution concentration ( $\sim 10^{-7}$ – $10^{-3}$ M), and surface loading ( $\sim 0.3$ – $3.0 \mu\text{mol m}^{-2}$ ). Mechanical modeling using the charge distribution approach revealed the formation of both monodentate and bidentate PMG complexes, each in two protonation states. PMG adsorption is dominated (>60 %) by the formation of a bidentate complex having a protonated amino group that deprotonates at high pH and low loading, aligning with previously published ATR-FTIR analyses. Monodentate complexes are less abundant and maintain a protonated amino group over the entire pH range. In addition, the phosphonate group becomes protonated at low pH and high loading. DFT calculations support the role of protons in the surface speciation. The obtained model was able to predict the solution concentration of PMG and its strong pH dependency over the full range in our experiments. Our study provides a new mechanistic and quantitative understanding of PMG binding to goethite, which enables improved predictions of the fate and transport of PMG in and towards natural waters, and provides a framework for optimizing the removal efficiency of PMG with metal (hydr)oxides.

## 1. Introduction

Currently, glyphosate (N-phosphonomethyl glycine, PMG) is globally the most widely used herbicide in agriculture for weed control (Duke, 2020). This herbicide is non-selective and is applied post-emergence since the uptake is primarily foliar (Blake and Pallett, 2018).

Chemically, PMG is a rather atypical herbicide since it is a highly polar molecule due to charging through the deprotonation of its carboxylic (–COOH) and phosphonate (–PO(OH)<sub>2</sub>) functional groups, and protonation of the amino (–NH) group (Barja and Afonso, 1998). At circumneutral pH, PMG is zwitterionic and net negatively charged. It strongly binds to positively charged metal (hydr)oxides in soils, sediments and suspended particulate matter, which controls the mobility, bio-availability, and fate of PMG in the environment (Aparicio et al.,

2013; Borggaard and Gimsing, 2008; Gimsing et al., 2004; Sun et al., 2019).

Because of this strong interaction, PMG is supposed to be immobile in soils and to have a low risk of contaminating the surrounding environment after agricultural application (Borggaard and Gimsing, 2008). However, increasing concerns have been raised about PMG pollution of ground-, surface-, and marine waters in agricultural basins, where it is detected in the liquid phase as well as bound to the sediment and suspended particulate matter (Aparicio et al., 2013; Daouk et al., 2013; Feltracco et al., 2022; Mac Loughlin et al., 2020; Ronco et al., 2016; Zhang et al., 2024). This is often attributed to run-off events or preferential flow routes (Vereecken, 2005). Besides agricultural sources, urban PMG which enters natural water systems via wastewater has been identified as another major source of PMG contamination in rivers (Botta et al., 2009; Hanke et al., 2010; Kolpin et al., 2006; Schwientek

\* Corresponding author.

E-mail address: [bram.geysels@wur.nl](mailto:bram.geysels@wur.nl) (B. Geysels).

<https://doi.org/10.1016/j.watres.2024.123031>

Received 14 November 2024; Received in revised form 19 December 2024; Accepted 20 December 2024

Available online 21 December 2024

0043-1354/© 2024 The Author(s). Published by Elsevier Ltd. This is an open access article under the CC BY license (<http://creativecommons.org/licenses/by/4.0/>).

et al., 2024). In traditional wastewater treatment plants, PMG is partly removed by sorption to iron (hydr)oxides in the activated sludge (Poiger et al., 2020). Adsorption on specific metal (hydr)oxides, including goethite (Doyle et al., 2023; Zhang et al., 2022) and magnetite (Lita et al., 2023; Park et al., 2019), is often proposed as a wastewater remediation technique for PMG (Georgin et al., 2024). Improved understanding of the adsorption process of PMG on metal (hydr)oxides allows optimization of these processes and prediction the influence of the reaction medium.

The most common crystalline iron (hydr)oxide in soils and sediments is goethite (FeOOH). Therefore, PMG binding to this iron oxyhydroxide has been studied extensively (Ahmed et al., 2018; Arroyave et al., 2017, 2016; Azimzadeh et al., 2024; Azimzadeh and Martínez, 2024; Day et al., 1997; Dideriksen and Stipp, 2003; Gimsing, 2001; Waiman et al., 2016, 2013). PMG binds mainly through inner-sphere complexation of the phosphonate group (Barja and Afonso, 2005; Sheals et al., 2002; Yan and Jing, 2018). However, there is no consensus about the denticity and protonation status of the functional groups of the PMG surface complexes, while this is pivotal for understanding and modeling its pH- and concentration-dependent adsorption behavior, and the interaction with competing ions in the environment.

The PMG surface speciation has been frequently studied with attenuated total reflection Fourier-transformed infrared (ATR-FTIR) spectroscopy (Barja and Afonso, 2005; Orcelli et al., 2018; Sheals et al., 2002; Yan and Jing, 2018). Published ATR-FTIR spectra are consistent and reliable in the various publications and there is a clear agreement on the experimental spectra measured. Lacking, however, is a solid basis for the interpretation of these spectra. Indicative of this knowledge gap are the widely varying interpretations and conclusions reached in the different publications while discussing near-identical spectra. This illustrates the inherent uncertainties in the interpretation arising from the deconvolution of the spectra, peak assignments, and observed absorbances. Sheals et al. (2002) proposed that PMG binds mainly through monodentate complex formation having either a protonated or a deprotonated amino group with only a minor contribution of binuclear bidentate (BB) complex formation, based on ATR-FTIR and X-ray photoelectron spectroscopy (XPS). On the other hand, Barja and Afonso (2005) proposed the formation of a combination of two mononuclear monodentate (MM) surface complexes and a binuclear bidentate (BB) surface complex, all having a protonated amino group. Including molecular orbital/density functional theory (MO/DFT) calculations, Yan and Jing (2018) suggested that a mononuclear bidentate (MB) surface complex may form as well.

Besides the varying interpretations, the surface speciation of PMG is not only dependent on pH, but also on its surface loading, and additionally, on the surface structure of the studied goethite that may differ in crystal face contributions and surface sites (Livi et al., 2023).

Gaining more insights into the surface speciation of PMG and its environmental implications may therefore benefit from applying additional tools. Mechanism-based surface complexation modeling (SCM) enables the translation of macroscopic adsorption data to insights on a molecular scale, hereby identifying surface complexes and understanding the variation in binding modes as a function of pH and loading. It can be particularly informative when the model is constrained by the interfacial charge distributions of the surface complexes, derived from MO/DFT geometry optimizations combined with a realistic surface model for the metal (hydr)oxide (Hiemstra and Van Riemsdijk, 1996). A major advantage of mechanistic sorption models is, as they are based on an accurate description of the underlying intrinsic chemical and electrostatic interactions, the high predictive power as they are robust and applicable outside of the conditions used in the development of the model. A similar approach has been successful in understanding the adsorption of metal ions (Mendez and Hiemstra, 2020; Van Eynde et al., 2022) and oxyanions (Antelo et al., 2005; Hiemstra et al., 2007; Van Eynde et al., 2020) but has not yet been applied to multiply charged organic chemicals that are relatively large in size and, concordantly,

may distribute their charged functional groups over multiple locations in the interface.

In earlier attempts to model PMG binding to goethite, a single surface site approach was used, and all charge at the functional groups of the PMG molecule was reduced to a single point charge that was placed at the surface (Barja and Afonso, 2005; Sheals et al., 2002), which can be seen as an unrealistic simplification. This shortcoming was addressed by Jonsson et al. (2008) who advocated the use of a more realistic electrical double layer (EDL) model by introducing a Stern layer and the use of an interfacial charge distribution of the adsorbed PMG ions, combined with a multiple reactive site approach based on the surface structure of goethite. The authors applied the charge distribution and multisite (CD-MUSIC) approach (Hiemstra and Van Riemsdijk, 1996) to an extensive dataset of Sheals et al. (2002) and could describe the data well. However, as our analysis in the current study will show, the applied interfacial charge distribution is physically unrealistic.

The goal of the present study is to develop a coherent and physically realistic interpretation of PMG binding and its pH- and loading-dependent surface speciation on goethite as a representative crystalline iron (hydr)oxide in terrestrial and aquatic systems. For this purpose, we will perform adsorption experiments over a wide pH and concentration range using a well-crystallized goethite combined with previously published adsorption data (Jonsson et al., 2008). The data will be used to derive a coherent set of parameters to mechanistically describe the adsorption and surface speciation of PMG using the CD-MUSIC model. Our model development will be guided and constrained by previously published spectroscopic observations, limiting the considered surface complexes, supplemented with MO/DFT optimization of the geometry, from which the interfacial charge distribution of the involved surface complexes to the surface will be derived and theoretical IR spectra will be computed. Collectively, it will provide a consistent adsorption model providing further insights into the environmental fate of PMG.

## 2. Material & methods

### 2.1. Materials

Well-crystallized goethite ( $A_{\text{BET}} = 94 \text{ m}^2 \text{ g}^{-1}$ ) was prepared and characterized in an earlier study (Weng et al., 2007). A  $12.1 \text{ g L}^{-1}$  stock suspension in a  $0.01 \text{ M NaNO}_3$  was prepared and stored at  $\text{pH} \sim 7$  under  $\text{N}_2$  to avoid contamination with atmospheric  $\text{CO}_2$  and specific care was taken to minimize carbonation during the experiments.

Glyphosate-isopropylamine stock solution (46 % PMG), provided by Bayer, was diluted to  $0.8 \text{ M PMG}$  in  $0.01 \text{ M NaNO}_3$ . The purity of the PMG stock was checked using High-Performance Liquid Chromatography Mass Spectroscopy (HPLC-MS). The total PMG concentration corresponded to the total P concentration measured using High-Resolution Inductively Coupled Plasma Mass Spectroscopy (HR-ICP-MS, Thermo Scientific Element 2). No other compounds could be detected in observable amounts.

### 2.2. PMG adsorption experiments

Adsorption envelopes were obtained for 8 different initial PMG concentrations at a single goethite concentration of  $0.60 \text{ g L}^{-1}$  in a background electrolyte solution of  $0.01 \text{ M NaNO}_3$ . For each initial PMG level, 10 batches were prepared in which the pH was adjusted by adding  $0.01 \text{ M HNO}_3$  or  $\text{NaOH}$ . The total volume of each system was adjusted to  $10.0 \text{ mL}$  by adding  $0.01 \text{ M NaNO}_3$ .

The prepared PMG-goethite systems were placed in a horizontal shaker and equilibrated at a constant temperature of  $20 \text{ }^\circ\text{C}$  for 24 hours. Preliminary experiments indicated no further decrease in PMG solution concentrations after this time, and no degradation of PMG could be observed as assessed by HPLC-MS. After equilibration,  $1 \text{ mL}$  aliquots were taken from each system and transferred into a microcentrifuge tube

for high-speed centrifugation (20 min at 18000 g) as using a low centrifugation volume substantially improved the phase separation. From the supernatant, 0.5 mL aliquots were diluted 1:20 using 0.14 M HNO<sub>3</sub> followed by measuring P with ICP-MS-HR. Centrifugation efficiency was verified by additionally measuring Fe in the supernatant, which was found to be lower than 0.1 % of total Fe. The potential contribution of PMG bound to this remaining Fe was calculated to be below 1 % of the measured P concentration in solution. Equilibrium pH was measured in the remaining 9 mL of the non-centrifuged suspension.

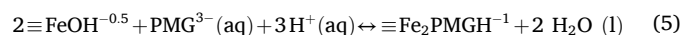
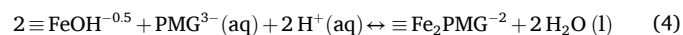
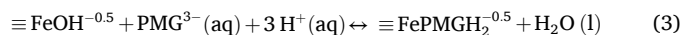
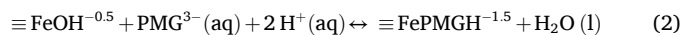
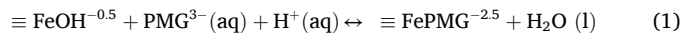
### 2.3. Adsorption model

For our well-crystallized goethite, singly ( $\equiv\text{FeOH}^{-0.5}$ ) and triply ( $\equiv\text{Fe}_3\text{O}^{-0.5}$ ) coordinated surface groups are considered in the model. The site densities ( $N_s$ ), affinity constants ( $\log K$ ) for  $\text{H}^+$ ,  $\text{Na}^+$ ,  $\text{NO}_3^-$  (Hiemstra et al., 2010) as well as the capacitance values for the extended Stern layer model are given in Table S1 (Supporting Information, SI). The solution speciation constants of PMG (Table S2) are based on Barja and Afonso (1998).

### 2.4. Surface complex formation

Our interpretation of the published IR spectra (see Section 3.6) follows the consensus that PMG forms inner-sphere complexes via the

phosphonate group and that the  $-\text{COO}^-$  group does not protonate in our considered pH range (Barja and Afonso, 2005; Sheals et al., 2002; Yan and Jing, 2018). Based on this, five surface reactions can be defined covering the monodentate and bidentate modes of binding, according to:



where  $\text{PMG}^{3-}(\text{aq})$  is the fully deprotonated glyphosate complex in solution. The structures of the surface complexes formed by the above reactions that are used in the final model, optimized by MO/DFT, are represented in Fig. 1 and Figure S8, and will be henceforth referred to with their abbreviations M, MH, MH<sub>2</sub>, B and BH for Eq. (1)–(5) respectively.

In our model, no distinct mononuclear bidentate complexes were considered, as it would require the formation of an energetically unfavorable four-membered ring (Barja and Afonso, 2005). In addition,

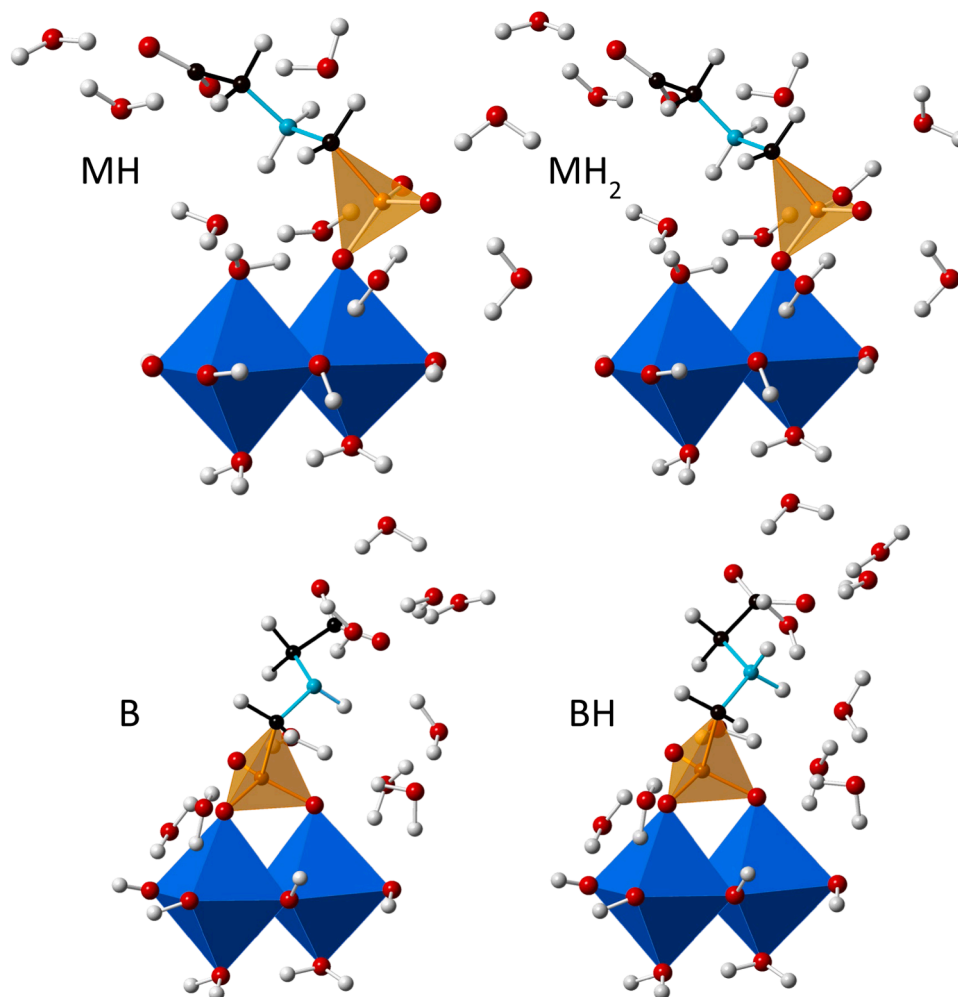


**Fig. 1.** Four surface complexes used in the final model: monodentate with a protonated amino and a deprotonated phosphonate (MH), monodentate with both protonated amino and phosphonate (MH<sub>2</sub>), bidentate with a deprotonated amino (B) and bidentate with protonated amino (BH). The structures were optimized by MO/DFT, using the 6-31+G\*\* basis set with the  $\omega$ B97M-V functional. The abbreviations MH, MH<sub>2</sub>, B, and BH refer to the surface complexes formed in Eqs. (2)–(5) respectively.

binding sites allowing mononuclear bidentate complexes are limited on goethite unless it contains many crystal defects (Livi et al., 2023); because we used a well-crystallized goethite in our experiments, mononuclear bidentate complexes can only be of minor importance (Hiemstra and Van Riemsdijk, 1996).

## 2.5. Calculation of charge distribution coefficients

The geometry of the various surface complexes was optimized using molecular orbital (MO) calculations applying density functional theory (DFT) (Fig. 1) with various functionals (see Section 2.7). Applying the Brown bond valence approach (Brown and Altermatt, 1985), the charge attribution to the surface ( $\Delta z_0$ ) was calculated and a small correction for interfacial dipole orientation of water molecules was included (Hiemstra and Van Riemsdijk, 2006).

In our modeling approach, the charge attribution to the Stern layers was derived by parameter optimization. The charge attribution to the outer Stern plane ( $\Delta z_2$ ) will be mainly controlled by the contribution of the  $-\text{COO}^-$  ligand, which remains unprotonated for all considered surface complexes. To minimize the number of adjustable parameters, a common value for  $\Delta z_2$  was used for all surface complexes. The attribution to the inner Stern plane ( $\Delta z_1$ ) was calculated, using the fitted common value for  $\Delta z_2$ , from the definition  $\Delta z_1 = \Delta z_{\text{tot}} - \Delta z_0 - \Delta z_2$  (Hiemstra and Van Riemsdijk, 2006) in which  $\Delta z_{\text{tot}}$  equals the sum of the charge of  $\text{PMG}^{3-}$  and  $\text{H}^+$  defined in the formation reactions, consequently, the charge attributions for all complexes to both Stern layers are determined by a single free parameter.

## 2.6. Parameter optimization

For our own experimental data, parameters were optimized by minimizing the difference between the calculated and measured percentage of adsorbed PMG. For the literature data (Jonsson et al., 2008), the surface loading ( $\Gamma$ ) was used as the evaluation scale since the adsorption data was only reported at that scale. Modeling was performed using ECOSAT v4.9 software (Keizer and Van Riemsdijk, 1998) combined with FIT v2.581 (Kinniburgh, 1993) for parameter optimization.

## 2.7. DFT calculations

MO/DFT was used to optimize cluster geometry, and to perform IR frequency and thermochemical calculations using Spartan'20. Functionals with increasing levels of theory were applied (B3LYP, EDF2,  $\omega$ B97X-D, and  $\omega$ B97M-V). The latter two functionals include range separation and dispersion, and outperform other functionals in energy and bond lengths calculations (Mardirossian and Head-Gordon, 2017). Unrestricted, open shell calculations were done, defining appropriately 5 unpaired electrons per Fe in the cluster (high-spin), and we applied the split-valence 6-31+G\*\* basis function that includes diffuse (+) and polarization (\*) functions. Glyphosate was explicitly hydrated with 7-8 water molecules and additionally, the C-PCM for solvation in water was applied.

## 3. Results & discussion

### 3.1. Initial modeling of literature data

Jonsson et al. (2008) have modeled the PMG adsorption using a charge distribution approach, applying the Basic Stern double layer option, and determined the CD coefficients by parameter optimization. The authors assumed the formation of two monodentate surface complexes (M and MH) that differ in the protonation of the amino group, following the suggestion of Sheals et al. (2002). The validity of their reported CD coefficients can be checked by comparing the fitted parameters with a Pauling bond valence distribution approximation. In

this approach, an equal distribution of the valence charge of the  $-\text{PO}_3^{2-}$  to the three oxygens is assumed, yielding a charge of  $-2/3 = -0.67$  v.u. per oxygen. In the formation reaction for both monodentate species, a proton (+1) is adsorbed to the surface hydroxyl to form  $\text{H}_2\text{O}$  (Eqs. (1) & (2)), leading to a CD coefficient of  $\Delta z_0 = +1 - 0.67 = +0.33$  v.u. for both monodentate complexes with unprotonated phosphonate.

For the MH surface complex (Eq. (2)), the fitted CD coefficients of Jonsson et al. (2008) were  $\Delta z_0 = +0.32$  v.u. and  $\Delta z_1 = -1.32$  v.u. This is in excellent agreement with the value from the Pauling bond valence approach where  $\Delta z_0 = +0.33$  v.u. and  $\Delta z_1 = \Delta z_{\text{tot}} - \Delta z_0 = -1.33$  v.u.

When the above Pauling bond valence approach is applied to the formation of the M surface complex (Eq. (1)), a  $\Delta z_0 = +0.33$  v.u. and  $\Delta z_1 = -2.33$  v.u. is obtained. However, the authors fitted  $\Delta z_0 = -0.2$  v.u. and  $\Delta z_1 = -1.8$  v.u. as CD values. This is not in agreement and highly unlikely as similar inner-sphere complexes of oxyanions, such as phosphate and arsenate (Antelo et al., 2005; Rahnemaie et al., 2007), have always been reported with positive  $\Delta z_0$  values. The negative value of  $\Delta z_0$  suggests a lack of positive charge in the formation reaction, for example in the form of an additional proton which would be used in the formation of a bidentate (B) surface complex. In addition, the fitted value of  $\Delta z_1 = -1.8$  v.u. for this species, determined by the observed electrostatic competition, suggests that there is a prevalent species present with a similar  $\Delta z_1$ . When we apply the Pauling bond valence theory to a bidentate species (B), two oxygens involved in a bidentate complex would each attribute  $-2/3$  charge to the surface. When considering the two co-adsorbed protons forming  $\text{H}_2\text{O}$  (Eq. (4)), CD coefficients yield  $\Delta z_0 = +2 - 1.33 = +0.67$  v.u. and  $\Delta z_1 = -1.67$  v.u., the latter value being close to the fitted value of  $\Delta z_1 = -1.8$  v.u. These observations motivated us to reinterpret the adsorption data of Jonsson et al. (2008) with the inclusion of a bidentate surface complex.

In our initial approach, we assumed a combination of a monodentate (MH) and bidentate (B) inner-sphere complex and derived the following CD values from the MO/DFT optimized geometry:  $\Delta z_0 = +0.41$ ;  $\Delta z_1 + \Delta z_2 = -1.41$  v.u. for MH, and  $\Delta z_0 = +0.69$ ;  $\Delta z_1 + \Delta z_2 = -1.69$  v.u. for B. This approach resulted in an excellent description (Table S3, Figure S2,  $R^2 = 0.9997$ ) of the data. However, disagreements of the modeled surface speciation with spectroscopic observations (see Section 3.6) required this model to be reconsidered as well.

Calculation of the MH and B surface speciation (Figure S3) shows an almost complete transition of MH to B at a pH increase from 4 to 9. This is not in line with IR spectroscopy which suggests only minor changes when varying pH (Barja and Afonso, 2005; Yan and Jing, 2018). In addition, it should be noted that the B surface complex has a deprotonated amino group and is present throughout the entire pH range according to this model, while deprotonation of this group only occurs at a high pH according to ATR-FTIR spectroscopy (Sheals et al., 2002; Yan and Jing, 2018).

A potential reason for obtaining an inconsistent surface speciation might be the incompleteness of the dataset used for this initial modeling. In a considerable part of the data set (Jonsson et al., 2008), the added PMG is almost completely ( $\sim 100\%$ ) adsorbed and the corresponding solution concentrations were not reported. This part of the data shows no variation with pH and does not give insight into the corresponding solution concentration and surface speciation. Only at high pH and surface loading, the adsorption was  $< 100\%$  and varied with pH. Therefore, we have set up new adsorption experiments to provide a dataset with increased sensitivity to modeling. These data will be evaluated and discussed first before we return to the data set of Jonsson et al. (2008) in an attempt to unify both.

### 3.2. Modeling of new dataset

In the newly collected dataset, the surface loading ( $\Gamma$ ) shows a larger pH-dependent variation (Fig. 2c). The majority of the data points in our experiments have a fraction adsorbed between  $\sim 20\%$  and  $\sim 80\%$  of the added amount of PMG (Fig. 2a), and the equilibrium concentrations

varied over  $>3$  orders of magnitude (Fig. 2b). The surface loading ( $\Gamma$ ) varied by about a factor of 10 between  $\sim 0.35$  and  $\sim 3.5 \mu\text{mol m}^{-2}$  (Fig. 2c).

The final model predictions presented in Fig. 2 are the result of a model-fitting approach in which the number of chosen surface species was gradually increased. We started with the two surface species, MH and B, that provided a good prediction of the literature dataset. However, our newly collected data cannot be described well with this 2-species approach and showed systematic errors (Table S4, Figure S4,  $r^2=0.9810$ ). The quality of the fit could be improved substantially by introducing a protonated bidentate BH ( $r^2=0.9929$ ), revealing the dominance of this BH species at low and neutral pH. The quality of the resulting fit was good but showed some systemic deviations at low pH

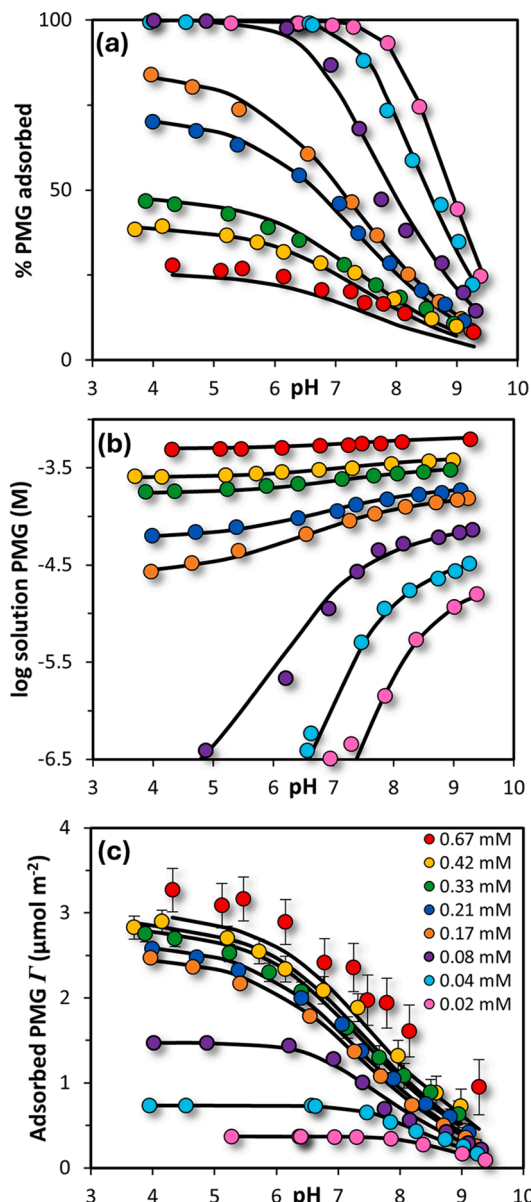


**Fig. 2.** (a) Percentage adsorbed PMG, (b) logarithm of the equilibrium concentration in solution, and (c) surface loading  $\Gamma$  of PMG as a function of pH in goethite systems of  $0.6 \text{ g l}^{-1}$  ( $94 \text{ m}^2 \text{ g}^{-1}$ ) with  $0.01 \text{ M NaNO}_3$  as background electrolyte. Solid lines represent the model predictions using the parameters determined in this study (Table 1). Datapoints of solution concentration below the level of detection are not shown in (b). Error bars in (c) represent the resulting variation in adsorbed PMG when assuming an uncertainty of the measured PMG solution concentration of 3% (see main text).

and high surface loading. This may be due to the protonation of the MH surface complex. The introduction of  $\text{MH}_2$  further improved the quality of the fit ( $r^2=0.9943$ ). The inclusion of  $\text{MH}_2$  only provides a small improvement, as the species' presence is minor in our range, but is included in the final model because of the chemical consistency (see Sections 3.3, 3.4). No contribution of the fully unprotonated monodentate surface complex (M) could be revealed. The final set of adsorption parameters is given in Table 1.

Although the parameter optimization was performed using only the percentage adsorbed as the scale for evaluation (Fig. 2a), the model provides an excellent prediction of the solution concentration (Fig. 2b), which can be considered the most important factor in an environmental assessment context, being relevant for the mobility and bio-availability of PMG. The lower end of our concentration range ( $10^{-6}$  -  $10^{-7} \text{ M}$ ) is typically found in surface- (Peruzzo et al., 2008) and pore waters (Mencaroni et al., 2023) in or near intensive agricultural soil systems, illustrating the practical relevance of our model.

Our data and model predictions can also be presented in terms of surface loading (Fig. 2c). At the highest initial PMG concentration (0.67 mM), some deviation is noticeable. We have repeated the experiment for the two highest PMG additions (SI Section S5) where we found that the observed deviation is within the observed variability of the experiment (Figure S5). The large deviation in surface loading corresponds to a deviation of  $\sim 3\%$  in the measured solution concentration and it does not affect the fitted model parameters significantly (Table S5, S6), therefore the repeated data was not included when fitting the final model. The large deviation in surface loading for this total concentration is the consequence of error propagation of smaller deviations in the measured solution concentration. To indicate this, an uncertainty of 3% in the measured PMG solution concentrations has been assumed to calculate the error bars in Fig. 2c, showing a larger uncertainty for high concentrations, and indicating that the model predictions fall within this experimental uncertainty.

### 3.3. Surface speciation of PMG on goethite

The model parameters of Table 1 can be used to calculate the surface speciation of PMG adsorbed to goethite as a function of pH and the initial PMG concentration of the system. In Fig. 3, the surface concentration is represented using the absolute scale (Fig. 3a, c) and relative scale (Fig. 3b, d).

Our modeling suggests that PMG is predominantly bound as a bidentate (BH and B) species over the entire pH range. The monodentate complexes (MH and  $\text{MH}_2$ ) also contribute significantly to the surface speciation but are a minor fraction. The bidentate species (BH and B) differ in the protonation of the amino group. Deprotonation of the  $-\text{NH}_2$

**Table 1**

Model parameters ( $\pm$  standard error) for complexation of PMG with the singly coordinated  $\equiv\text{FeOH}^{0.5}$  surface groups of goethite. The surface charge attributions ( $\Delta z_0$ ) were derived from the MO/DFT optimized geometries of the various complexes. The individual log K values and the common value for  $\Delta z_2$  were fitted on the fraction adsorbed as shown in Figure 2a ( $R^2=0.9943$ ,  $\text{RMSE}=2.38\%$ ,  $n=80$ ). The applied capacitance values for the extended Stern layer model are  $C_1=0.83 \text{ F m}^{-2}$  and  $C_2=0.74 \text{ F m}^{-2}$  (Weng et al., 2007). All other surface equilibria concerning  $\text{H}^+$ ,  $\text{Na}^+$ , and  $\text{NO}_3^-$  are specified in Table S1.

Complex	Name	Reaction	$\Delta z_0$	$\Delta z_1^*$	$\Delta z_2$	$\Delta z_{\text{tot}}$	log K
$\equiv\text{FePMGH}$	MH	Eq. (2)	0.28	-0.54	-0.74	-1	23.57
				$\pm 0.07$	$\pm 0.07$		$\pm 0.33$
$\equiv\text{FePMGH}_2$	$\text{MH}_2$	Eq. (3)	0.41	0.33	-0.74	0	28.66
				$\pm 0.07$	$\pm 0.07$		$\pm 0.74$
$\equiv\text{Fe}_2\text{PMG}$	B	Eq. (4)	0.69	-0.95	-0.74	-1	24.36
				$\pm 0.07$	$\pm 0.07$		$\pm 0.20$
$\equiv\text{Fe}_2\text{PMGH}$	BH	Eq. (5)	0.75	-0.01	-0.74	0	32.60
				$\pm 0.07$	$\pm 0.07$		$\pm 0.30$

\* Calculated from the charge balance  $\Delta z_1 = \Delta z_{\text{tot}} - \Delta z_0 - \Delta z_2$ .

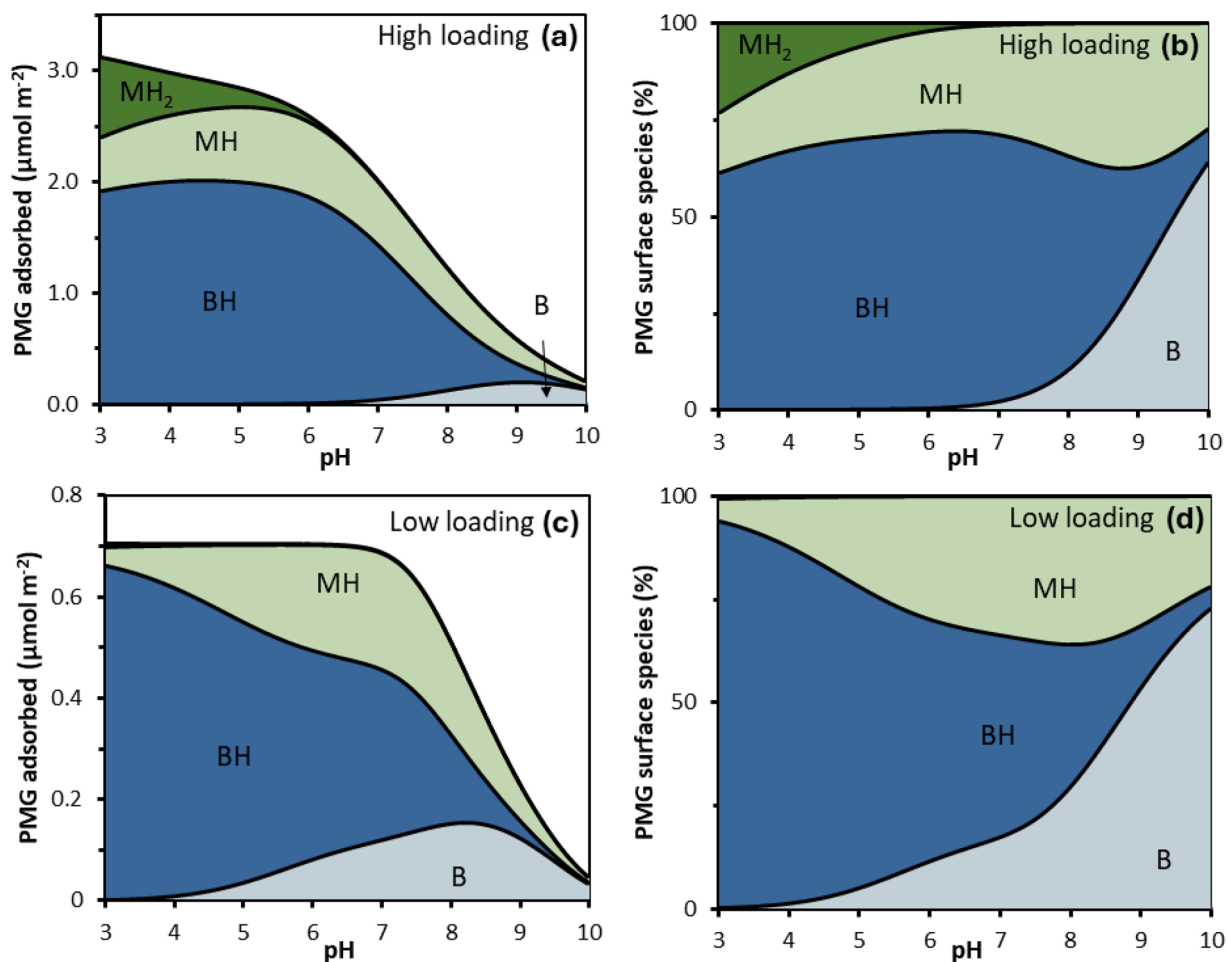


**Fig. 3.** Surface speciation and corresponding relative contributions of PMG adsorbed to goethite in 0.01 M NaNO<sub>3</sub> as a function of pH, modeled using the parameters of Table 1 for 0.6 g L<sup>-1</sup> goethite (94 m<sup>2</sup> g<sup>-1</sup>) systems having 0.67 mM (a, b) or 0.04 mM total PMG (c, d). Only B has a deprotonated amino, where it is protonated for all other species. MH<sub>2</sub> has an additional proton on the phosphonate (Fig. 1).

group becomes important at high pH and this process is stronger at low surface loadings, as less negative interface potential is introduced by the negative charge of the adsorbed PMG molecules. The amino groups of both monodentate complexes (MH<sub>2</sub> and MH) are protonated over the entire range. The monodentate MH complex may accept an additional proton, bound to the -PO<sub>3</sub> group, forming MH<sub>2</sub> (Fig. 3a). The MH<sub>2</sub> surface species is only formed at a combination of a low pH and high surface loading. The latter factor causes a decrease of the electrostatic potential in the Stern layer, stimulating the proton adsorption.

The possibility for the monodentate surface complexes to form a strong hydrogen bond with the neighboring surface group, as found for silicic acid (Hiemstra, 2018; Wang et al., 2018), was explored in our study by MO/DFT geometry optimization (SI Section S6). While the final H-bond formed is weak and the charge contribution of these bonds falls within the uncertainty of the fitted CD coefficients, in exploring this possibility, we observed a spontaneous shift of the proton bound to -PO<sub>3</sub> of the MH<sub>2</sub> surface complex to the surface site in the MO/DFT optimization. This indicates that the proton affinity of the ≡FeOH<sup>-0.5</sup> group of the cluster (Hiemstra and Van Riemsdijk, 1996; Zhang et al., 2021) is likely to be distinctly higher than that of the -PO<sub>3</sub> group.

### 3.4. Proton affinity of the surface complexes

Our modeling shows that the protonation is an essential aspect of the surface speciation of PMG (Fig. 3). At low pH, the transformation from MH to MH<sub>2</sub> is observed, while at higher pH, BH deprotonates and forms B. The proton affinity constants of both reactions can be calculated by

combining the formation constants (Table 1) of both complexes involved. The proton affinity of MH ( $MH + H^+(aq) \leftrightarrow MH_2$ ,  $\log K_H = 5.1 \pm 1.1$ ) describes the protonation of the phosphonate group, while the proton affinity of B ( $B + H^+(aq) \leftrightarrow BH$ ,  $\log K_H = 8.2 \pm 0.5$ ) concerns the protonation of the amino group and is consequently higher.

These values are supported by our thermochemical calculations using MO/DFT. We calculated the Gibbs free energy which we used for a thermochemical interpretation of proton transfer reactions. We avoid the need for the absolute Gibbs free energy of a proton, which is notoriously difficult to calculate, by considering scenarios of an equivalent atomic composition.

For the proton transfer reaction of  $B + MH_2 \leftrightarrow BH + MH$ , we find  $\log K_a$  values of 4.1, 3.8 and 3.1, applying DFT with B3LYP, ωB97X-D, and ωB97M-V respectively. The experimental  $\log K$  for this proton exchange reaction is  $\log K_a = 3.2$ , obtained by combining the equilibrium constants of all four complexes (Table 1). This value is best reproduced with MO/DFT/ωB97M-V. The calculated  $\log K$  values are positive, implying that the combination of BH and MH are more stable, in agreement with the dominance of these species in our modeled speciation (Fig. 3).

Following a similar approach for the reaction  $BH + M \leftrightarrow B + MH$ , we predict  $\log K_b = 2.5, 3.1$  and  $2.9$  using B3LYP, ωB97X-D, and ωB97M-V respectively. The positive  $\log K$  shows that the combination of B and MH is more stable than BH and M, which is also found with our CD modeling as no contribution of the M surface species is found. In the above reaction, a proton is transferred from the -NH<sub>2</sub> group of BH to the same group of M. The positive value of  $\log K_b$  indicates that an unprotonated

amine is more favorable for the bidentate than for the monodentate. This can be explained by B having an additional interaction of its  $-\text{PO}_3$  with Fe, decreasing the proton affinity of the  $-\text{NH}$  group further in the chain.

We can explore this approach further by using our experimental  $\log K_{\text{H}}$  value for  $\text{B} + \text{H}^+(\text{aq}) \leftrightarrow \text{BH}$ ,  $\log K_{\text{B}/\text{BH}} = 8.2$  which we consider the most reliable experimental protonation constant due to the prevalence of the bidentate species, as a reference. Using this reaction combined with the reaction  $\text{B} + \text{MH}_2 \leftrightarrow \text{BH} + \text{MH}$  with  $\log K_{\text{a}} = 3.1$  as calculated with MO/DFT/ $\omega\text{B97M-V}$ , we can calculate  $\log K_{\text{MH}/\text{MH}_2} = \log K_{\text{B}/\text{BH}} - \log K_{\text{a}} = 5.1$ , corresponding with our experimental value. Similarly, by combining the bidentate protonation constant with the reaction  $\text{BH} + \text{M} \leftrightarrow \text{B} + \text{MH}$ , with  $\log K_{\text{b}} = 2.9$ , we find  $\log K_{\text{M}/\text{MH}} = \log K_{\text{B}/\text{BH}} + \log K_{\text{b}} = 11.1$ . This high proton affinity can explain the absence of M in the surface speciation in our pH range.

A realistic assessment of absolute values for the Gibbs free energy of protonation, is notoriously difficult and requires more advanced approaches (Bursch et al., 2022; Malloum et al., 2021; Mardirossian and Head-Gordon, 2017; Zhang et al., 2021). Using our experimental  $\log K_{\text{B}/\text{BH}}$  as a reference is equivalent to using in the protonation reactions a Gibbs free energy of  $-1119.6 \text{ kJ mol}^{-1}$  for  $\text{H}^+(\text{aq})$ . This value is equal to the mean ( $-1119.6 \pm 1.2 \text{ kJ mol}^{-1}$ ) value derived with high-level quantum chemical modeling (Ishikawa and Nakai, 2016; Ridley et al., 2019). On the other hand, this theoretical value is at the higher end compared to a broader collection of theoretical and experimental values, typically being  $\sim 1100 \pm 15 \text{ kJ mol}^{-1}$  for  $\text{H}^+(\text{aq})$  (Malloum et al., 2021). Despite this deviation in absolute energy, our relative approach of thermochemical analysis seems to provide reliable information due to error cancelation (Bursch et al., 2022) and the outcomes strongly support our CD modeling of PMG adsorption.

### 3.5. Interfacial charge distribution and conformation of PMG surface complexes

The charge distribution coefficients (Table 1), calculated from MO/DFT optimized geometries ( $\Delta z_0$ ) and fitting ( $\Delta z_1$  &  $\Delta z_2$ ), describe the charge allocation of the functional groups  $-\text{PO}_3^-$ ,  $-\text{NH}_2^+$  and  $-\text{COO}^-$  that carry the charge. The CD coefficients thus provide insights into the conformation of the surface complexes and the positioning of the functional groups.

To reduce the number of adjustable parameters, a common value of  $\Delta z_2$  was used for all considered surface species, assuming only the deprotonated  $-\text{COO}^-$  would contribute charge to the outer Stern layer. Our model reveals that a significant amount of charge ( $\Delta z_2 = -0.74 \pm 0.07 \text{ v.u.}$ ) is present at the outer Stern plane. This plane is located at  $\sim 0.7\text{--}0.8 \text{ nm}$  distance from the goethite surface (Hiemstra and Van Riemsdijk, 2006). According to MO/DFT geometry optimization, an outstretched PMG molecule has about the same length ( $\sim 0.7 \text{ nm}$ ), which suggests that the adsorbed molecule tends to stretch and move the  $-\text{COO}^-$  group away from the surface. An outstretched conformation is supported by the absence of direct interactions between the amino or carboxylate group and the surface as reported based on ATR-FTIR spectroscopy (see Section 3.6).

The fitted value of the  $\Delta z_2$  charge is slightly less than the charge of the  $-\text{COO}^-$  group. Multiple factors may have caused this, such as the precise orientation of the ligand, a redistribution of charge along the chain, and/or H-bond formation between the  $-\text{NH}_2^+$  group and the  $-\text{COO}^-$ . Exploring the latter factor, the model was refitted with a separate  $\Delta z_2$  parameter for the B complex ( $\Delta z_{2,\text{B}}$ ), which has an unprotonated  $-\text{NH}$  group. Within the uncertainty, no change in the fitted parameters was found ( $\Delta z_{2,\text{B}} = -0.88 \pm 0.61 \text{ v.u.}$  and  $\Delta z_{2,\text{BH,MH,MH}_2} = -0.75 \pm 0.08 \text{ v.u.}$ ) and no improvement to the overall fit was observed.

### 3.6. IR spectroscopy

Our model results (Fig. 3) can be compared with the outcome of spectroscopic studies, comprising ATR-FTIR (Barja and Afonso, 2005;

Orcelli et al., 2018; Sheals et al., 2002; Yan and Jing, 2018) and XPS (Sheals et al., 2002), concerning the vibrational behavior of the  $-\text{COO}$ ,  $-\text{NH}$ , and  $-\text{PO}_3$  functional groups. To assist interpretation of the experimental spectra, we calculated theoretical IR spectra using MO/DFT. Yan and Jing (2018) used a similar approach, which we extend and improve upon by including the non-protonated species B and M, and using multiple functionals. A full discussion of the collected theoretical spectra and interpretation of the experimental spectra from literature is provided in the supporting information (SI Section S7), here, we provide only the main conclusions.

The first observation concerns the  $-\text{COO}^-$  group. In the ATR-FTIR spectra of adsorbed PMG (Sheals et al., 2002; Yan and Jing, 2018), an invariable vibrational band at  $1400 \text{ cm}^{-1}$  is found in the pH range 4–9, appointed to symmetric  $-\text{COO}^-$  stretching. For PMG in solution, a band is found at the same wavelength, which is absent at pH 1.5 i.e. when the  $-\text{COOH}$  group is protonated, and where a vibrational band at  $1750 \text{ cm}^{-1}$  is present (Sheals et al., 2001; Yan and Jing, 2018). The consistent presence of the  $1400 \text{ cm}^{-1}$  band and absence of a  $1750 \text{ cm}^{-1}$  band in the experimental spectra of adsorbed PMG confirms the absence of protonation of the  $-\text{COO}^-$ , fully aligning with our CD modeling, which shows this group remains deprotonated in the considered pH range and attributes most of its negative charge to the outer Stern layer. Our MO/DFT calculated spectra show a fairly consistent band at  $1400 \text{ cm}^{-1}$  for all species, and no features around  $1750 \text{ cm}^{-1}$  (Figure S12).

MO/DFT calculations show that the asymmetric stretching of the  $-\text{COO}^-$  group is affected by the protonation state of the amino group (Table S9). Dissolved PMG exhibits a complete transition of the corresponding spectral band from  $1610 \text{ cm}^{-1}$  to  $1570 \text{ cm}^{-1}$  in the pH range 9–12 i.e. following the deprotonation of the  $-\text{NH}_2$  (Sheals et al., 2001; Yan and Jing, 2018). Adsorbed PMG features a single band around  $\sim 1600 \text{ cm}^{-1}$  which splits into a  $\sim 1580 \text{ cm}^{-1}$  and  $\sim 1630 \text{ cm}^{-1}$  band at pH  $\sim 9$  (Sheals et al., 2002; Yan and Jing, 2018) and simultaneously intensifies, indicating a partial deprotonation of the  $-\text{NH}_2$ . The deprotonation of  $-\text{NH}_2$  of adsorbed PMG is supported by our CD model, showing a transformation from BH to B with increasing pH (Fig. 3). It is further supported by X-ray photoelectron spectroscopy (XPS) data of Sheals et al. (2002). This is in direct opposition to the conclusions of Yan and Jing (2018), who did not consider surface complexes with a deprotonated amine, and assign the changes in the spectra at the transition of pH 9 to 8 to an unlikely protonation of the  $-\text{PO}_3$ .

In the  $900\text{--}1200 \text{ cm}^{-1}$  region, the spectral bands are the results of  $-\text{PO}_3$  stretching, with two fairly consistent major experimental bands laying near  $\sim 1140\text{--}1120 \text{ cm}^{-1}$  and  $\sim 985\text{--}975 \text{ cm}^{-1}$  (Barja and Afonso, 2005; Orcelli et al., 2018; Sheals et al., 2002; Yan and Jing, 2018). The two bands show a slight shift towards lower wavenumbers with increasing pH (Barja and Afonso, 2005; Orcelli et al., 2018; Sheals et al., 2002; Yan and Jing, 2018) and decreasing loading (Barja and Afonso, 2005; Sheals et al., 2002). According to our calculations (Figure S12), the wavenumbers of both major peaks shift to lower wavenumbers following the order  $\text{MH}_2 > \text{MH} > \text{BH} > \text{B}$ .

In the low-frequency range of this region ( $\sim 1000 \text{ cm}^{-1}$ ), most experimental spectra show a major peak around  $\sim 980 \text{ cm}^{-1}$  with a prominent shoulder around  $1010\text{--}1020 \text{ cm}^{-1}$  (Barja and Afonso, 2005; Orcelli et al., 2018; Sheals et al., 2002; Yan and Jing, 2018). Our calculated  $-\text{PO}_3$  stretching peaks in this range (Table S10) suggest that the major peak can be assigned to BH, while the shoulder can be assigned to MH. This is consistent with our modeled speciation where we identify BH as the dominant species with MH being secondary in most of the pH range (Fig. 3). With increasing pH, where BH partly deprotonates to form B, as indicated by our model and the spectroscopic observations concerning the amino group, no separate vibrational band can be observed for this species, however, the major peak at  $\sim 980 \text{ cm}^{-1}$  shows a shift towards lower wavelengths (Barja and Afonso, 2005; Orcelli et al., 2018; Sheals et al., 2002; Yan and Jing, 2018). Corresponding to our model, this potentially indicates that the major peak comprises  $-\text{PO}_3$  vibrations of both B and BH surface complexes, with

increasing contribution of B as pH increases.

The calculated frequencies in the high-frequency range ( $\sim 1100\text{ cm}^{-1}$ , Table S11), independently of the chosen functional, are systematically lower than found experimentally (Barja and Afonso, 2005; Orcelli et al., 2018; Sheals et al., 2002; Yan and Jing, 2018), showing a limitation of the applied approach. This prevents us from assigning the peaks absolutely, but we can interpret the relative changes. Following the findings from the low-frequency range which confirmed BH as the dominant species, we can reasonably assign the most prominent band to BH, potentially with a contribution of B. This allows us to use the relative shift of the calculated frequencies to assign the remaining experimental bands. When applying this strategy to the deconvoluted spectra of Orcelli et al. (2018), the major band shifts from  $\sim 1450\text{ cm}^{-1}$  to  $\sim 1250\text{ cm}^{-1}$  with increasing pH, which could be interpreted as BH with increasing contribution of B. A minor band around  $\sim 1165\text{ cm}^{-1}$  is found throughout the pH range, thus potentially indicating the presence of the MH species.

The discrepancy between the calculated and experimental frequencies for the  $-\text{PO}_3$  stretching frequencies could be caused by several reasons (see SI Section S7). We consider the most likely explanation that the structuring of water molecules near the surface (Hiemstra and Van Riemsdijk, 2006) could impact the vibrational frequencies of the ligands near the surface, which is not accounted for in MO/DFT simulations. This is motivated by the observation that the vibrational frequencies of the functional groups further away from the surface ( $-\text{NH}$  and  $-\text{COO}$ ) show a very good correspondence between the experimental and theoretical wavelengths. Nevertheless, our approach utilizing the relative changes in wavelengths provides support to the proposed surface speciation.

Our model identified a  $\text{MH}_2$  species which cannot be confirmed by spectroscopy as the contribution is low and, following our model, would be absent in most of the conditions where the spectra are collected. The spectra show no indication of the presence of the M species.

### 3.7. A unified model interpretation

With the insights obtained from modeling our dataset, we have revisited the dataset of Jonsson et al. (2008), which can be well described using our 4-species approach (Figure S13, Table S12,  $r^2=0.9996$ ). Moreover, the obtained surface speciation is quite similar to the speciation found for our goethite, with similar proton affinity constants of the surface complexes ( $\log K_{\text{H,MH}\rightarrow\text{MH}_2} = 6.0 \pm 0.3$  and  $\log K_{\text{H,B}\rightarrow\text{BH}} = 7.7 \pm 0.1$ ), and consistent with the spectroscopic analysis. However, no common set of affinity constants can be obtained as the charge development of the goethite of Jonsson et al. (2008) is significantly higher, which is reflected in a higher value for the inner Stern layer capacitance ( $C_1=0.99\text{ Fm}^{-2}$ ) compared to our goethite ( $C_1=0.84\text{ Fm}^{-2}$ ), which may be due to the presence of defects in the crystal structure in the former (Martínez et al., 2023).

In our modeling of the data of Jonsson et al. (2008), the common parameter for the charge attribution to the outer Stern layer ( $\Delta z_2$ ) was similarly obtained by fitting. The value derived from this dataset was  $-0.98 \pm 0.03$ , slightly higher than the value of  $-0.74 \pm 0.07$  obtained for our data set. Both datasets, however, support the presence of a significant charge contribution of the  $-\text{COO}^-$  group to the outer Stern plane. This highlights the importance of having a complete and consistent molecular understanding for extrapolating a SCM to other datasets.

## 4. Conclusions and implications

The current research is the first to give a consistent, mechanistic, quantitative and generic view on glyphosate binding to goethite over a wide range of environmental conditions, interpreted with a state-of-the-art surface complexation model constrained by quantum chemical calculations. The molecular interpretation of the model aligns well with thermochemical DFT calculations, independent spectroscopic

observations from literature and previous studies of glyphosate adsorption on goethite. The effect of pH and surface loading are well predicted by our model and indicate a correct distinction between the intrinsic affinity of the surface species and the electrostatic interactions. The complete and consistent speciation with a realistic description of the electrostatic effect of our model enables multicomponent predictive modeling in other environmental conditions at varying glyphosate concentrations, pH, ionic strength and competitors.

Since iron (hydr)oxides control the availability, mobility, and degradation of glyphosate in aquatic and terrestrial systems, our developed model contributes to a generic and quantitative interpretation of the fate of glyphosate in the natural environment. This mono-component, single-surface model is an important first step toward a multi-component, multi-surface model that predicts glyphosate adsorption in complex, water-metal (hydr)oxide systems such as soils, sediments, and water bodies. It also provides a useful tool for optimizing PMG removal in wastewater treatment with varying compositions. The proposed model is a starting point in further investigation of glyphosate binding to other materials, such as ferrihydrite and magnetite, and in the presence of ubiquitous compounds that could impact glyphosate adsorption by co-adsorption (e.g. Ca and Mg) or competition (e.g. phosphate and natural organic matter).

### CRedit authorship contribution statement

**Bram Geysels:** Writing – original draft, Visualization, Methodology, Investigation, Formal analysis, Data curation, Conceptualization. **Tjisse Hiemstra:** Writing – review & editing, Visualization, Formal analysis, Conceptualization. **Jan E. Groenenberg:** Writing – review & editing, Supervision, Conceptualization. **Rob N.J. Comans:** Writing – review & editing, Supervision, Conceptualization.

### Declaration of competing interest

The authors declare that they have no known competing financial interests or personal relationships that could have appeared to influence the work reported in this paper.

### Acknowledgment

The research was funded by Invite GmbH. We thank Ronald Vermeer, Stefan Herrmann, Roman Heumann and Werner Hoheisel for guidance and counsel, and Peter Nobels for the ICP measurements.

### Supplementary materials

Supplementary material associated with this article can be found, in the online version, at doi:10.1016/j.watres.2024.123031.

### Data availability

Data will be made available on request.

### References

- Ahmed, A.A., Leinweber, P., Kühn, O., 2018. Unravelling the nature of glyphosate binding to goethite surfaces by *ab initio* molecular dynamics simulations. *Phys. Chem. Chem. Phys.* 20, 1531–1539. <https://doi.org/10.1039/C7CP06245A>.
- Antelo, J., Avena, M., Fiol, S., López, R., Arce, F., 2005. Effects of pH and ionic strength on the adsorption of phosphate and arsenate at the goethite–water interface. *J. Colloid Interface Sci.* 285, 476–486. <https://doi.org/10.1016/j.jcis.2004.12.032>.
- Aparicio, V.C., De Gerónimo, E., Marino, D., Primost, J., Carriquiriborde, P., Costa, J.L., 2013. Environmental fate of glyphosate and aminomethylphosphonic acid in surface waters and soil of agricultural basins. *Chemosphere* 93, 1866–1873. <https://doi.org/10.1016/j.chemosphere.2013.06.041>.
- Arroyave, J.M., Waiman, C.C., Zanini, G.P., Avena, M.J., 2016. Effect of humic acid on the adsorption/desorption behavior of glyphosate on goethite. Isotherms and kinetics. *Chemosphere* 145, 34–41. <https://doi.org/10.1016/j.chemosphere.2015.11.082>.

- Arroyave, J.M., Waiman, C.C., Zanini, G.P., Tan, W., Avena, M.J., 2017. Desorption rate of glyphosate from goethite as affected by different entering ligands: hints on the desorption mechanism. *Environ. Chem.* 14, 288. <https://doi.org/10.1071/EN17004>.
- Azimzadeh, B., Martínez, C.E., 2024. Unraveling the role of polysaccharide-goethite associations on glyphosate' adsorption-desorption dynamics and binding mechanisms. *J. Colloid Interface Sci.* 653, 1283–1292. <https://doi.org/10.1016/j.jcis.2023.09.141>.
- Azimzadeh, B., Nicholson, L.K., Martínez, C.E., 2024. In the presence of the other: how glyphosate and peptide molecules alter the dynamics of sorption on goethite. *Sci. Total Environ.* 912, 169264. <https://doi.org/10.1016/j.scitotenv.2023.169264>.
- Barja, B.C., Dos Santos Afonso, M., 2005. Aminomethylphosphonic acid and glyphosate adsorption onto goethite: a comparative study. *Environ. Sci. Technol.* 39, 585–592. <https://doi.org/10.1021/es035055q>.
- Barja, B.C., Dos Santos Afonso, M., 1998. An ATR-FTIR study of glyphosate and its Fe (III) complex in aqueous solution. *Environ. Sci. Technol.* 32, 3331–3335. <https://doi.org/10.1021/es9800380>.
- Blake, R., Pallett, K., 2018. The environmental fate and ecotoxicity of glyphosate. *Outlook Pest Manag.* 29, 266–269. [https://doi.org/10.1564/v29\\_dec\\_08](https://doi.org/10.1564/v29_dec_08).
- Borggaard, O.K., Gimsing, A.L., 2008. Fate of glyphosate in soil and the possibility of leaching to ground and surface waters: a review. *Pest Manag. Sci.* 64, 441–456. <https://doi.org/10.1002/ps.1512>.
- Botta, F., Lavison, G., Couturier, G., Alliot, F., Moreau-Guigon, E., Fauchon, N., Guery, B., Chevreuil, M., Blanchoud, H., 2009. Transfer of glyphosate and its degradate AMPA to surface waters through urban sewerage systems. *Chemosphere* 77, 133–139. <https://doi.org/10.1016/j.chemosphere.2009.05.008>.
- Brown, I.D., Altermatt, D., 1985. Bond-valence parameters obtained from a systematic analysis of the Inorganic Crystal Structure Database. *Acta Crystallogr. B Struct. Sci.* 41, 244–247. <https://doi.org/10.1107/S0108768185002063>.
- Bursch, M., Mewes, J., Hansen, A., Grimme, S., 2022. Best-Practice DFT protocols for basic molecular computational chemistry\*\*. *Angew. Chem. Int. Ed.* 61. <https://doi.org/10.1002/anie.202205735>.
- Daouk, S., De Alencastro, L.F., Pfeifer, H.-R., 2013. The herbicide glyphosate and its metabolite AMPA in the Lavaux vineyard area, western Switzerland: proof of widespread export to surface waters. Part II: the role of infiltration and surface runoff. *J. Environ. Sci. Health Part B* 48, 725–736. <https://doi.org/10.1080/03601234.2013.780548>.
- Day, G.M., Hart, B.T., McKelvie, I.D., Beckett, R., 1997. Influence of natural organic matter on the sorption of biocides onto goethite. II. Glyphosate. *Environ. Technol.* 18, 781–794. <https://doi.org/10.1080/09593331808616597>.
- Dideriksen, K., Stipp, S.L.S., 2003. The adsorption of glyphosate and phosphate to goethite: a molecular-scale atomic force microscopy study. *Geochim. Cosmochim. Acta* 67, 3313–3327. [https://doi.org/10.1016/S0016-7037\(02\)01369-8](https://doi.org/10.1016/S0016-7037(02)01369-8).
- Doyle, S., Garvey, M., Fowley, C., 2023. Removal of Glyphosate from water through adsorption onto Goethite Nanoparticles. *Environ. Nanotechnol. Monit. Manag.* 20, 100839. <https://doi.org/10.1016/j.enmm.2023.100839>.
- Duke, S.O., 2020. Glyphosate: environmental fate and impact. *Weed Sci.* 68, 201–207. <https://doi.org/10.1017/wsc.2019.28>.
- Feltracco, M., Barbaro, E., Morabito, E., Zangrando, R., Piazza, R., Barbante, C., Gambaro, A., 2022. Assessing glyphosate in water, marine particulate matter, and sediments in the Lagoon of Venice. *Environ. Sci. Pollut. Res.* 29, 16383–16391. <https://doi.org/10.1007/s11356-021-16957-x>.
- Georgin, J., Stracke Pflingsten Franco, D., Gindri Ramos, C., Nguyen Tran, H., Benettayeb, A., Imanova, G., Ali, I., 2024. Recent advances in removing glyphosate herbicide and its aminomethylphosphonic acid metabolite in water. *J. Mol. Liq.* 402, 124786. <https://doi.org/10.1016/j.molliq.2024.124786>.
- Gimsing, A.L., 2001. Effect of KCl and CaCl<sub>2</sub> as background electrolytes on the competitive adsorption of glyphosate and phosphate on goethite. *Clays Clay Miner.* 49.
- Gimsing, A.L., Borggaard, O.K., Bang, M., 2004. Influence of soil composition on adsorption of glyphosate and phosphate by contrasting Danish surface soils. *Eur. J. Soil Science* 55, 183–191. <https://doi.org/10.1046/j.1365-2389.2003.00585.x>.
- Hanke, I., Wittmer, I., Bischofberger, S., Stamm, C., Singer, H., 2010. Relevance of urban glyphosate use for surface water quality. *Chemosphere* 81, 422–429. <https://doi.org/10.1016/j.chemosphere.2010.06.067>.
- Hiemstra, T., 2018. Ferrihydrite interaction with silicate and competing oxyanions: geometry and Hydrogen bonding of surface species. *Geochim. Cosmochim. Acta* 238, 453–476. <https://doi.org/10.1016/j.gca.2018.07.017>.
- Hiemstra, T., Antelo, J., Rahnemaie, R., Riemsdijk, W.H.V., 2010. Nanoparticles in natural systems I: the effective reactive surface area of the natural oxide fraction in field samples. *Geochim. Cosmochim. Acta* 74, 41–58. <https://doi.org/10.1016/j.gca.2009.10.018>.
- Hiemstra, T., Barnett, M.O., Van Riemsdijk, W.H., 2007. Interaction of silicic acid with goethite. *J. Colloid Interface Sci.* 310, 8–17. <https://doi.org/10.1016/j.jcis.2007.01.065>.
- Hiemstra, T., Van Riemsdijk, W.H., 2006. On the relationship between charge distribution, surface hydration, and the structure of the interface of metal hydroxides. *J. Colloid Interface Sci.* 301, 1–18. <https://doi.org/10.1016/j.jcis.2006.05.008>.
- Hiemstra, T., Van Riemsdijk, W.H., 1996. A surface structural approach to ion adsorption: the charge distribution (CD) model. *J. Colloid Interface Sci.* 179, 488–508. <https://doi.org/10.1006/jcis.1996.0242>.
- Ishikawa, A., Nakai, H., 2016. Quantum chemical approach for condensed-phase thermochemistry (III): accurate evaluation of proton hydration energy and standard hydrogen electrode potential. *Chem. Phys. Lett.* 650, 159–164. <https://doi.org/10.1016/j.cplett.2016.03.004>.
- Jonsson, C.M., Persson, P., Sjöberg, S., Loring, J.S., 2008. Adsorption of glyphosate on goethite ( $\alpha$ -FeOOH): surface complexation modeling combining spectroscopic and adsorption data. *Environ. Sci. Technol.* 42, 2464–2469. <https://doi.org/10.1021/es070966b>.
- Keizer, M.G., Van Riemsdijk, W.H., 1998. ECOSATFITmanual.pdf.
- Kinniburgh, D.G., 1993. Technical Report WD/93/23 FIT User Guide.
- Kolpin, D.W., Thurman, E.M., Lee, E.A., Meyer, M.T., Furlong, E.T., Glassmeyer, S.T., 2006. Urban contributions of glyphosate and its degradate AMPA to streams in the United States. *Sci. Total Environ.* 354, 191–197. <https://doi.org/10.1016/j.scitotenv.2005.01.028>.
- Lita, A.L., Hidayat, E., Mohamad Sarbani, N.M., Harada, H., Yonemura, S., Mitoma, Y., Herviyanti, Gusmini, 2023. Glyphosate removal from water using biochar based coffee husk loaded Fe<sub>3</sub>O<sub>4</sub>. *Water (Basel)* 15, 2945. <https://doi.org/10.3390/w15162945>.
- Livi, K.J.T., Villalobos, M., Ramasse, Q., Brydson, R., Salazar-Rivera, H.S., 2023. Surface site density of synthetic goethites and its relationship to atomic surface roughness and crystal size. *Langmuir* 39, 556–562. <https://doi.org/10.1021/acs.langmuir.2c02818>.
- Mac Loughlin, T.M., Peluso, M.L., Aparicio, V.C., Marino, D.J.G., 2020. Contribution of soluble and particulate-matter fractions to the total glyphosate and AMPA load in water bodies associated with horticulture. *Sci. Total Environ.* 703, 134717. <https://doi.org/10.1016/j.scitotenv.2019.134717>.
- Malloum, A., Fifen, J.J., Conradie, J., 2021. Determination of the absolute solvation free energy and enthalpy of the proton in solutions. *J. Mol. Liq.* 322, 114919. <https://doi.org/10.1016/j.molliq.2020.114919>.
- Mardirossian, N., Head-Gordon, M., 2017. Thirty years of density functional theory in computational chemistry: an overview and extensive assessment of 200 density functionals. *Mol. Phys.* 115, 2315–2372. <https://doi.org/10.1080/00268976.2017.1333644>.
- Martínez, R.J., Villalobos, M., Loredó-Jasso, A.U., Cruz-Valladares, A.X., Mendoza-Flores, A., Salazar-Rivera, H., Cruz-Romero, D., 2023. Towards building a unified adsorption model for goethite based on direct measurements of crystal face compositions: I. Acidity behavior and As(V) adsorption. *Geochim. Cosmochim. Acta* 354, 252–262. <https://doi.org/10.1016/j.gca.2023.06.021>.
- Mencaroni, M., Longo, M., Cardinali, A., Lazzaro, B., Zanin, G., Dal Ferro, N., Morari, F., 2023. Glyphosate and AMPA dynamics during the transition towards conservation agriculture: drivers under shallow groundwater conditions. *Soil Tillage Res.* 229, 105659. <https://doi.org/10.1016/j.still.2023.105659>.
- Mendez, J.C., Hiemstra, T., 2020. High and low affinity sites of ferrihydrite for metal ion adsorption: data and modeling of the alkaline-earth ions Be, Mg, Ca, Sr, Ba, and Ra. *Geochim. Cosmochim. Acta* 286, 289–305. <https://doi.org/10.1016/j.gca.2020.07.032>.
- Orcelli, T., Di Mauro, E., Urbano, A., Valezi, D.F., Da Costa, A.C.S., Zaia, C.T.B.V., Zaia, D.A.M., 2018. Study of Interaction between glyphosate and goethite using several methodologies: an environmental perspective. *Water Air Soil Pollut.* 229, 150. <https://doi.org/10.1007/s11270-018-3806-1>.
- Park, H., May, A., Portilla, L., Dietrich, H., Münch, F., Rejek, T., Sarcletti, M., Banspach, L., Zahn, D., Halik, M., 2019. Magnetite nanoparticles as efficient materials for removal of glyphosate from water. *Nat. Sustain.* 3, 129–135. <https://doi.org/10.1038/s41893-019-0452-6>.
- Peruzzo, P.J., Porta, A.A., Ronco, A.E., 2008. Levels of glyphosate in surface waters, sediments and soils associated with direct sowing soybean cultivation in north pampasic region of Argentina. *Environ. Pollut.* 156, 61–66. <https://doi.org/10.1016/j.envpol.2008.01.015>.
- Poiger, T., Keller, M., Buerge, I.J., Balmer, M.E., 2020. Behavior of glyphosate in wastewater treatment plants. *Chimia (Aarau)* 74, 156. <https://doi.org/10.2533/chimia.2020.156>.
- Rahnemaie, R., Hiemstra, T., Van Riemsdijk, W.H., 2007. Geometry, charge distribution, and surface speciation of phosphate on goethite. *Langmuir* 23, 3680–3689. <https://doi.org/10.1021/la062965n>.
- Ridley, M.K., Lischka, H., Tunega, D., Aquino, A.J.A., 2019. Solvent effect on Al(III) hydrolysis constants from density functional theory. *Mol. Phys.* 117, 1507–1518. <https://doi.org/10.1080/00268976.2019.1567846>.
- Ronco, A.E., Marino, D.J.G., Abellano, M., Almada, P., Apartin, C.D., 2016. Water quality of the main tributaries of the Paraná Basin: glyphosate and AMPA in surface water and bottom sediments. *Environ. Monit. Assess.* 188, 458. <https://doi.org/10.1007/s10661-016-5467-0>.
- Schwientek, M., Rügner, H., Haderlein, S.B., Schulz, W., Wimmer, B., Engelbart, L., Bieger, S., Huhn, C., 2024. Glyphosate contamination in European rivers not from herbicide application? *Water Res.* 263, 122140. <https://doi.org/10.1016/j.watres.2024.122140>.
- Sheals, J., Persson, P., Hedman, B., 2001. IR and EXAFS spectroscopic studies of glyphosate protonation and copper(II) complexes of glyphosate in aqueous solution. *Inorg. Chem.* 40, 4302–4309. <https://doi.org/10.1021/ic000849g>.
- Sheals, J., Sjöberg, S., Persson, P., 2002. Adsorption of glyphosate on goethite: molecular characterization of surface complexes. *Environ. Sci. Technol.* 36, 3090–3095. <https://doi.org/10.1021/es010295w>.
- Sun, M., Li, H., Jaisi, D.P., 2019. Degradation of glyphosate and bioavailability of phosphorus derived from glyphosate in a soil-water system. *Water Res.* 163, 114840. <https://doi.org/10.1016/j.watres.2019.07.007>.
- Van Eynde, E., Hiemstra, T., Comans, R.N.J., 2022. Interaction of Zn with ferrihydrite and its cooperative binding in the presence of PO<sub>4</sub>. *Geochim. Cosmochim. Acta* 320, 223–237. <https://doi.org/10.1016/j.gca.2022.01.010>.
- Van Eynde, E., Mendez, J.C., Hiemstra, T., Comans, R.N.J., 2020. Boron adsorption to ferrihydrite with implications for surface speciation in soils: experiments and

- modeling. *ACS Earth Space Chem.* 4, 1269–1280. <https://doi.org/10.1021/acsearthspacechem.0c00078>.
- Vereecken, H., 2005. Mobility and leaching of glyphosate: a review. *Pest Manag. Sci.* 61, 1139–1151. <https://doi.org/10.1002/ps.1122>.
- Waiman, C.V., Arroyave, J.M., Chen, H., Tan, W., Avena, M.J., Zanini, G.P., 2016. The simultaneous presence of glyphosate and phosphate at the goethite surface as seen by XPS, ATR-FTIR and competitive adsorption isotherms. *Colloids Surf. A Physicochem. Eng. Asp.* 498, 121–127. <https://doi.org/10.1016/j.colsurfa.2016.03.049>.
- Waiman, C.V., Avena, M.J., Regazzoni, A.E., Zanini, G.P., 2013. A real time in situ ATR-FTIR spectroscopic study of glyphosate desorption from goethite as induced by phosphate adsorption: effect of surface coverage. *J. Colloid Interface Sci.* 394, 485–489. <https://doi.org/10.1016/j.jcis.2012.12.063>.
- Wang, X., Kubicki, J.D., Boily, J.-F., Waychunas, G.A., Hu, Y., Feng, X., Zhu, M., 2018. Binding geometries of silicate species on ferrihydrite surfaces. *ACS Earth Space Chem.* 2, 125–134. <https://doi.org/10.1021/acsearthspacechem.7b00109>.
- Weng, L., Van Riemsdijk, W.H., Hiemstra, T., 2007. Adsorption of humic acids onto goethite: effects of molar mass, pH and ionic strength. *J. Colloid Interface Sci.* 314, 107–118. <https://doi.org/10.1016/j.jcis.2007.05.039>.
- Yan, W., Jing, C., 2018. Molecular insights into glyphosate adsorption to goethite gained from ATR-FTIR, two-dimensional correlation spectroscopy, and DFT study. *Environ. Sci. Technol.* 52, 1946–1953. <https://doi.org/10.1021/acs.est.7b05643>.
- Zhang, Q., Li, Y., Kroeze, C., Xu, W., Gai, L., Vitsas, M., Ma, L., Zhang, F., Strokal, M., 2024. A global assessment of glyphosate and AMPA inputs into rivers: over half of the pollutants are from corn and soybean production. *Water Res.* 261, 121986. <https://doi.org/10.1016/j.watres.2024.121986>.
- Zhang, X., Zhang, J., Peng, Y., Wu, X., Li, M., Wen, H., Sun, Z., Ye, J., Hua, Y., 2022. Synergistic removal of glyphosate and U(VI) from aqueous solution by goethite: adsorption behaviour and mechanism. *J. Radioanal. Nucl. Chem.* 331, 1807–1819. <https://doi.org/10.1007/s10967-022-08223-2>.
- Zhang, Y., Liu, X., Cheng, J., Lu, X., 2021. Interfacial structures and acidity constants of goethite from first-principles Molecular Dynamics simulations. *Am. Mineral.* 106, 1736–1743. <https://doi.org/10.2138/am-2021-7835>.